Available online at www.sciencedirect.com
SCIENCE DIRECT®
Continental Shelf Research 25 (2005) 1583–1603
CONTINENTAL SHELF RESEARCH
www.elsevier.com/locate/csr

# Modelling the dispersion of radionuclides by a river plume: Application to the Rhone river

R. Periáñez

*Dpto. Física Aplicada I, E.U. Ingeniería Técnica Agrícola, Universidad de Sevilla. Ctra. Utrera km 1, 41013 Sevilla, Spain*

Received 16 January 2004; received in revised form 25 January 2005; accepted 15 April 2005
Available online 14 June 2005

**Abstract**

A numerical model to simulate the transport of radionuclides in a river plume has been developed. The model solves the hydrodynamic equations, including baroclinic terms and a 1-equation turbulence model, suspended matter equations, including several particle sizes and deposition and erosion of sediments, and the radionuclide dispersion equations. The exchanges of radionuclides between water, suspended matter and bed sediments are described in terms of kinetic transfer coefficients. The dependence of these coefficients with water salinity is explicitly included in the model since in a river plume it changes from freshwater to seawater values. The model has been applied to the Rhone River plume, where radionuclides have been mainly discharged from a nuclear fuel reprocessing plant. Four particle sizes have been considered. Computed currents, salinity patterns, suspended sediment distributions and sedimentation rates are, in general, in agreement with observations. The model has been applied to simulate the transport of $^{125}$Sb, $^{137}$Cs and $^{239,240}$Pu in the river plume. The model provides realistic radionuclide distributions in water, suspended matter and bottom sediments. Other valuable information, as fractions of radionuclides in suspended particles and distribution coefficients, can also be provided by the model.


*Keywords:* Rhone River; Hydrodynamics; Sediment; Numerical modelling; Dispersion; Radionuclides

## 1. Introduction

In recent times there has been an increasing interest in the development of dynamic radionuclide dispersion models in the marine environment since they are useful instruments that can be used in the assessment of the radiological consequences of existing or planned routine discharges of radionuclides, as well as to determine the potential impacts of accidental discharges (Thiessen et al., 1999). An understanding of the processes that govern the fate of discharged radionuclides is also of interest, both from the political and the environmental point of view, since the knowledge of the dose received by the population in the future may be needed. Finally, useful oceanographic

*E-mail address:* rperianez@us.es.

0278-4343/$ - see front matter © 2005 Elsevier Ltd. All rights reserved.
doi:10.1016/j.csr.2005.04.001

information can be obtained by means of the application of marine radionuclide dispersion models (Prandle, 1984; Salomon et al., 1995). A general discussion on this point may be seen in Scott (2003). Also, some discussion on the interest of radionuclides as indicators of transport, deposition and resuspension processes may be seen in the book of Eisma (1993, p. 65), and references included there.

Radionuclide dispersion in the marine environment is governed by advective transport and turbulent diffusion (these processes being induced by tidal, wind and long-term residual currents), but radionuclides also suffer chemical processes like adsortion/desorption reactions between water and solid particles (suspended matter particles and bottom sediments) and are affected by other complex physical processes (like deposition of suspended particles on the bed and erosion of the bottom sediment). Due to computational limitations, the first radionuclide dispersion models were long-term models in which advective and diffusive transport was parameterized in terms of effective transfer coefficients (Abril and García-León, 1993; Nielsen, 1995; Nielsen et al., 1997; Gurbutt et al., 1988). Also, time steps used in these models were long enough to allow the description of adsorption/desorption reactions in terms of equilibrium distribution coefficients, $k_d$s.

More recently, dynamic models in which advective transport is explicitly calculated for tidally resolving computed currents have been developed. The treatment of adsorption/desorption has also been improved through the use of kinetic transfer coefficients. Thus, models can be applied to situations other than equilibrium conditions. This kind of model has been applied to estuaries (see, for instance, Periáñez et al., 1996a; Periáñez and Martínez-Aguirre, 1997; Margvelashvily et al., 1999; Periáñez, 2002) and the marine environment (for instance Piasecki, 1998; Periáñez, 1999, 2000; Aldridge et al., 2003; Goshawk et al., 2003; Smith et al., 2003; Nakano and Povinec, 2003). However, although some models have already been developed to study the water circulation in a river plume (Ruddick et al., 1995; Luyten et al., 1996; Estournel et al., 1997; Marsaleix et al., 1998; Cugier and Le Hir, 2002), none of them has been applied to simulate the transport of radionuclides from the river to the coastal area. This is an interesting problem since a complex intrusion process occurs when a freshwater input runs into marine waters. It mainly depends upon the interaction between the bouyancy induced momentum fluxes, which spread the freshwater offshore, and the turbulent dilution and dissipation mechanisms, which reduce density differences between the two water masses. Also, adsorption/desorption reactions are affected by salinity changes. The dependence of kinetic coefficients governing such reactions with salinity must be explicitly included in a model. Finally, the size spectra of suspended particles discharged by the river may be rather wide. A recent sensitivity study (Periáñez, 2004b) has indicated that model output is very sensitive to the suspended particle size used in the model. Thus, more realistic results should be obtained if several particle sizes are considered.

In this paper, a model for simulating the transport of radionuclides in a river plume is described and applied to the Rhone River plume, which introduces radionuclides released to the river into the Mediterranean Sea. The model domain covers all the river plume in the coastal area, where salinity changes from freshwater to seawater values. The artificial radionuclides reach the Rhone River through weathering of surface soils contaminated by atmospheric fallout and through the effluents from nuclear facilities: several nuclear power plants located along the river course and, mainly, from Marcoule nuclear fuel reprocessing plant (it ceased operations in 1997 but releases have continued since washing effluents are produced and discharged). In the case of the Rhone, the low mixing of the discharge waters gives rise to a well-identified surface plume in which a thin upper layer (1 or 2 m) is separated from the ambient seawater by a sharp density gradient. This plume extends 20 or 30 km offshore. Numerical modelling of these plumes is a difficult task that requires the inclusion of density differences in the full 3D hydrodynamic equations. The Rhone River gives the opportunity to test the behavior of radionuclide dispersion models, including a kinetic approach for the transfers between the liquid and solid phases, when

integrated with a detailed hydrodynamic model of a complex oceanographic system as a surface river plume.

It must be pointed out that some detailed models have already been developed to study the water circulation in the Rhone plume (Estournel et al., 1997, 2001; Marsaleix et al., 1998). Also, some models describe the transport of sediments in the plume (Kondrachoff et al., 1994; Estournel et al., 1997), although in a rather simple way. Indeed, only one particle size was considered in these references and deposition was not included. However, a radionuclide dispersion model for the plume, integrated with a hydrodynamic model and a detailed suspended sediment model, has not been described and tested before.

The model solves the full 3D hydrodynamic equations using a one-equation turbulence model for eddy viscosity. The water circulation is used to solve the suspended matter equations (one equation for each particle size), including processes of deposition and sediment erosion, and the radionuclide dispersion equations. The model is described in the following section. Then, results are presented.

## 2. Model description

The hydrodynamic, suspended sediments and radionuclide dispersion sub-models are presented in what follows.

### 2.1. Hydrodynamic model

The full 3D hydrodynamic equations including the terms corresponding to density gradients can be written in the hydrostatic and Boussinesq approximations as (Kowalick and Murty, 1993)

$$\frac{\partial \zeta}{\partial t}+\frac{\partial}{\partial x}\left[(h+\zeta)\int_{-h}^{\zeta} u\,\mathrm{d}z\right]+\frac{\partial}{\partial y}\left[(h+\zeta)\int_{-h}^{\zeta} v\,\mathrm{d}z\right]=0, \tag{1}$$

$$\frac{\partial u}{\partial t}+u\frac{\partial u}{\partial x}+v\frac{\partial u}{\partial y}-\Omega v+g\frac{\partial \zeta}{\partial x}+\frac{g}{\rho_0}\int_z^{\zeta}\frac{\partial \rho_w}{\partial x}\,\mathrm{d}z=\frac{\partial}{\partial z}\left(K\frac{\partial u}{\partial z}\right)+A\left(\frac{\partial^2 u}{\partial x^2}+\frac{\partial^2 u}{\partial y^2}\right), \tag{2}$$

$$\frac{\partial v}{\partial t}+u\frac{\partial v}{\partial x}+v\frac{\partial v}{\partial y}+\Omega u+g\frac{\partial \zeta}{\partial y}+\frac{g}{\rho_0}\int_z^{\zeta}\frac{\partial \rho_w}{\partial y}\,\mathrm{d}z=\frac{\partial}{\partial z}\left(K\frac{\partial v}{\partial z}\right)+A\left(\frac{\partial^2 v}{\partial x^2}+\frac{\partial^2 v}{\partial y^2}\right), \tag{3}$$

where the $z$ coordinate is measured upwards from the undisturbed sea level, $h$ is water depth, $\zeta$ is the displacement of the sea surface from the undisturbed level, $u$ and $v$ are the two components of the water velocity along the $x$- and $y$-axis, respectively, $\Omega$ is the Coriolis parameter, $\rho_w$ is water density, $\rho_0$ is a reference density, and $K$ and $A$ are the vertical and horizontal eddy viscosities, respectively.

The vertical component of the water velocity, $w$, is obtained from the continuity equation

$$\frac{\partial u}{\partial x}+\frac{\partial v}{\partial y}+\frac{\partial w}{\partial z}=0. \tag{4}$$

The water density is derived from a equation of state relating density to salinity (Kowalick and Murty, 1993)

$$\rho_w=\rho_0(1+\alpha S), \tag{5}$$

where $S$ is salinity and $\alpha=7.45\times10^{-4}$. As in Marsaleix et al. (1998), the effect of temperature on density is omitted for the sake of simplicity. Indeed, temperature differences between the Rhone River and the ambient seawater are small enough to consider that the bouyancy effects in the plume are represented only by the salinity gradients (Marsaleix et al., 1998). The reference salinity is taken as $\rho_0=998.9\,\mathrm{kg/m^3}$.

The salinity is determined from an advection–diffusion equation

$$\frac{\partial S}{\partial t}+u\frac{\partial S}{\partial x}+v\frac{\partial S}{\partial y}+w\frac{\partial S}{\partial z}=A\left(\frac{\partial^2 S}{\partial x^2}+\frac{\partial^2 S}{\partial y^2}\right)+\frac{\partial}{\partial z}\left(K\frac{\partial S}{\partial z}\right). \tag{6}$$

Vertical eddy viscosity is determined from the 1-equation turbulence model described in Davies and Hall (2000). This model has also been used in

Xing and Davies (1999) to simulate a river plume. The equation for the turbulent kinetic energy $E$ is

$$\frac{\partial E}{\partial t} = K\left\{\left(\frac{\partial u}{\partial z}\right)^2 + \left(\frac{\partial v}{\partial z}\right)^2\right\} + \beta_0 \frac{\partial}{\partial z}\left(K\frac{\partial E}{\partial z}\right) - \varepsilon + \frac{g}{\rho_0} K \frac{\partial \rho}{\partial z}. \quad (7)$$

The first term in the right-hand side of the equation represents generation of turbulence by the vertical shear, the second term is diffusion of turbulence and the last term is loss of turbulence by bouyancy (conversion of kinetic energy into potential energy). $\varepsilon$ represents dissipation of turbulence, that is written as

$$\varepsilon = C_1 E^{3/2}\ell, \quad (8)$$

where $\ell$ is a mixing length and $C_1$ a numeric coefficient. The vertical viscosity is finally written as a function of energy as

$$K = C_0 \ell E^{1/2} + \lambda_t, \quad (9)$$

where $C_0$ is a numeric coefficient and $\lambda_t$ is a background value of viscosity, that is the minimum possible value that it may have (Ruddick et al., 1995; Cugier and Le Hir, 2002). The values of the numeric constants appearing above are (Davies and Hall, 2000): $\beta_0 = 0.73$, $C_0 = C^{1/4}$, $C_1 = C_0^3$ and $C = 0.046$. The background viscosity is fixed as $\lambda_t = 10^{-4}\,\mathrm{m^2/s}$, which is the same value used in Ruddick et al. (1995).

The mixing length is derived from an algebraic expression (Davies and Hall, 2000)

$$\ell = \frac{1}{1/\ell_1 + 1/\ell_2} \quad (10)$$

with

$$\ell_1 = \kappa(z + z_0 + h)e^{\beta_1(z+h)/h}, \quad (11)$$

$$\ell_2 = \kappa(z_s - z), \quad (12)$$

where $\kappa = 0.4$ is the von Karman's constant, $\beta_1 = -2.0$ and $z_s$ and $z_0$ are the roughness lengths of the sea surface and bottom, respectively.

Boundary conditions have also to be provided for sea surface elevation, currents, salinity and kinetic energy. At the sea surface

$$\rho_0 K\left(\frac{\partial u}{\partial z}\right)_{z=\zeta} = F_s, \quad (13)$$

$$\rho_0 K\left(\frac{\partial v}{\partial z}\right)_{z=\zeta} = G_s, \quad (14)$$

where $F_s$ and $G_s$ are the components of the wind stress acting on the sea surface. For salinity, it is assumed that there is no flux through the sea surface and bottom

$$\left(\frac{\partial S}{\partial z}\right)_{z=-h,z=\zeta} = 0. \quad (15)$$

In the case of kinetic energy, the boundary condition at the sea surface is

$$E_{z=\zeta} = \frac{\tau_w}{\rho_0\sqrt{C_E}}, \quad (16)$$

where $\tau_w$ is the wind stress (solved in the components $F_s$ and $G_s$) and $C_E = 0.07$ (Estournel et al., 1997). If there is not wind, then the condition is (Davies and Hall, 2000)

$$\left(\frac{\partial E}{\partial z}\right)_{z=\zeta} = 0. \quad (17)$$

At the sea bottom, boundary conditions are

$$E_{z=-h} = \frac{\tau_b}{\rho_0\sqrt{C_E}}, \quad (18)$$

where $\tau_b$ is the bottom stress, solved in components $F_b$ and $G_b$, and $C_E = 0.07$ as in Estournel et al. (1997). For the currents,

$$\rho_0 K\left(\frac{\partial u}{\partial z}\right)_{z=-h} = F_b, \quad (19)$$

$$\rho_0 K\left(\frac{\partial v}{\partial z}\right)_{z=-h} = G_b. \quad (20)$$

The two components of the bottom stress are written using a quadratic friction law

$$F_b = \rho_0 k u\sqrt{u^2+v^2}, \quad G_b = \rho_0 k v\sqrt{u^2+v^2}, \quad (21)$$

where $k$ is a friction coefficient to be obtained after a calibration exercise.

A no-flux condition is applied along land boundaries. A radiation condition in the form of

Orlanski (1976) is applied along open boundaries for the water velocity component that is normal to the boundary:

$$\frac{\partial \xi}{\partial t} + c\frac{\partial \xi}{\partial n} = 0, \tag{22}$$

where $n$ is the direction normal to the boundary, $\xi = u, v$ is the water velocity component to which the condition is applied and $c$ is the wave speed calculated as in Orlanski (1976). This condition has also been used in Marsaleix et al. (1998). Surface elevations should be prescribed along open boundaries to propagate tides inside the computational domain. However, as will be shown below, tides are neglected in the present model application and the radiation condition is also applied to surface elevations.

Boundary conditions at the river mouth are

$$S = 0 \tag{23}$$

that is the freshwater value and

$$q_l = \frac{Q}{ld}, \tag{24}$$

where $q_l$ is the water velocity in the direction of the outflow, $Q$ is the river discharge and $l$ and $d$ are the width of the river mouth and the thickness of the outflow water layer, respectively.

### 2.2. Suspended sediment model

The suspended sediment dynamic is governed by an advection–diffusion dispersion equation to which the settling, erosion and deposition terms are added. A number $N$ of particle grain sizes are considered in the model. Each particle size is represented by a concentration $m_i$. The equation for size $i$ is

$$\frac{\partial m_i}{\partial t} + u\frac{\partial m_i}{\partial x} + v\frac{\partial m_i}{\partial y} + (w - w_{s,i})\frac{\partial m_i}{\partial z} = A\left(\frac{\partial^2 m_i}{\partial x^2} + \frac{\partial^2 m_i}{\partial y^2}\right) + \frac{\partial}{\partial z}\left(K\frac{\partial m_i}{\partial z}\right), \tag{25}$$

where $w_{s,i}$ is the corresponding settling velocity for particle size $i$. The deposition and erosion terms are incorporated into the sea bed boundary condition of the equation. The deposition rate is written as in other modelling studies (see, for instance, Nicholson and O'Connor, 1986; Holt and James, 1999; Liu et al., 2002a; Lumborg and Windelin, 2003; Wu et al., 1998; Prandle et al., 2000; Cancino and Neves, 1999)

$$DP_i = w_{s,i} m_i(b)\left(1 - \frac{\tau_b}{\tau_{cd}}\right), \tag{26}$$

where $m_i(b)$ is particle concentration of size $i$ evaluated at the sea bottom and $\tau_{cd}$ is a critical deposition stress above which no deposition occurs since particles are maintained in suspension by water turbulence.

The settling velocity for each particle size is determined from Stokes's law

$$w_{s,i} = \frac{\rho - \rho_w}{\rho_w}\frac{gD_i^2}{18v}, \tag{27}$$

where $\rho$ and $D_i$ are suspended particle density and diameter, respectively, and $v$ is kinematic viscosity of water. It is also possible to include the process of aggregation in the model through a classic relationship in the form (Mehta, 1989; Clarke, 1995)

$$w_{s,i} = a_1 m_i^{a_2}. \tag{28}$$

This approach has been used in some suspended sediment models (Cancino and Neves, 1999; Clarke and Elliott, 1998; Nicholson and O'Connor, 1986; Lumborg and Windelin, 2003) and also in radionuclide dispersion models (Periáñez, 1999, 2000). Other authors (Estournel et al., 1997; Liu et al. 2002a, b; Jiang et al., 2000; Segschneider and Sundermann, 1998; Holt and James, 1999) directly calculate the settling velocity from Stokes's law. Tattersall et al. (2003) have used a mixed approach. At each time step the settling velocity resulting from Eq. (28) is calculated and compared with that obtained from Stokes's law. Then the higher value is used. Wu et al. (1998) use Eq. (28) or Stokes's law depending on the suspended matter concentration. Stokes's law has been used in this work due to the difficulty of finding appropriate values for $a_1$ and $a_2$ for each particle size. Moreover, Thill et al. (2001) have found that it is not clear that the aggregation process could play a role in enhancing settling at the Rhone River mouth.

The erosion rate is written in terms of the erodability constant (Liu et al. 2002a, b; Cancino and Neves, 1999; Prandle et al., 2000; Holt and James, 1999; Nicholson and O'Connor, 1986)

$$ER_i = Ef_i\left(\frac{\tau_b}{\tau_{ce}} - 1\right), \tag{29}$$

where $E$ is the erodability constant, $f_i$ gives the fraction of particles of size $i$ in the bed sediment and $\tau_{ce}$ is a critical erosion stress below which no erosion occurs. The model can also calculate sedimentation rates as the balance between the deposition and erosion terms.

Bed-load transport of coarse particles has not been included since radionuclides are essentially adsorbed on the fine particles (McKay and Walker, 1990). This approach has also been used in other models (for instance, Periáñez, 1999).

### 2.3. Dispersion of radionuclides

It is considered that the exchanges of radionuclides between the liquid and solid phases are governed by a single reversible reaction. Thus, the transfer from the liquid to the solid phase is governed by a kinetic coefficient $k_1$ and the inverse process by a kinetic coefficient $k_2$. It is known that actinide adsorption tends to be a surface phenomenon and will depend on the surface of particles per water volume unit at each point and time step. This quantity has been denoted as the exchange surface (Periáñez et al., 1996b; Periáñez and Martínez-Aguirre, 1997; Periáñez, 1999, 2000, 2002). Thus, the kinetic coefficient $k_{1,i}$ is written as:

$$k_{1,i} = \chi_1(S_{m,i} + S_{s,i}) = k_{11,i} + k_{12,i}, \tag{30}$$

where $S_m$ and $S_s$ are the exchange surfaces for suspended matter and bottom sediments respectively and $\chi_1$ is a parameter with the dimensions of a velocity denoted as the exchange velocity (Periáñez et al., 1996b; Periáñez and Martínez-Aguirre, 1997; Periáñez, 1999, 2000, 2002). The index $i = 1 \ldots N$ is used to represent each one of the particle sizes included in the model. Assuming spherical particles, the exchange surfaces are written as (see references cited above)

$$S_{m,i} = \frac{3m_i}{\rho R_i} \tag{31}$$

and

$$S_{s,i} = \frac{3Lf_i\phi}{R_i\Upsilon}, \tag{32}$$

where $R_i$ is particle radius, $L$ is the sediment mixing depth (the distance to which the dissolved phase penetrates the sediment), $\Upsilon$ is the thickness of the water layer above the bed sediments that interacts with them and $\phi$ is a correction factor that takes into account that part of the sediment particle surface may be hidden by other particles. For simplicity, it has been assumed that $\Upsilon$ is equal to the vertical grid size: $\Upsilon = \Delta z$. This formulation has been successfully used in all modelling works cited above.

The exchange velocity depends on salinity as in Laissaoui et al. (1998)

$$\chi_1 = \chi_1^0(1 - \delta), \tag{33}$$

where

$$\delta = \frac{S}{S + S_0}. \tag{34}$$

In these equations $\chi_1^0$ is the freshwater value of the exchange velocity and $S_0$ is the salinity value at which 50% of saturation occurs (Laissaoui et al., 1998). It must be noted that as salinity increases, the transfer of radionuclides to the solid phase decreases due to competition effects of radionuclides with ions dissolved in water. The relations given above have been tested through laboratory experiments (Laissaoui et al., 1998).

The kinetic coefficient $k_2$ is considered to be constant and to have the same value for all particle sizes.

Recent work has shown that a kinetic model involving 2 consecutive reversible reactions (2-step model) may be more appropriate than one consisting of a single (1-step) reversible reaction, specially for long (months) water–sediment contact times (Periáñez, 2004a). However, given the time scale of simulations that are carried out (several days), it is not expected that significant

differences between the 1-step and 2-step model appear in this case.

The equation that gives the time evolution of specific activity in the dissolved phase, $C_d$, is

$$\frac{\partial C_d}{\partial t} + u\frac{\partial C_d}{\partial x} + v\frac{\partial C_d}{\partial y} + w\frac{\partial C_d}{\partial z} = A\left(\frac{\partial^2 C_d}{\partial x^2} + \frac{\partial^2 C_d}{\partial y^2}\right) + \frac{\partial}{\partial z}\left(K\frac{\partial C_d}{\partial z}\right) - \sum_{i=1}^{N} k_{11,i}C_d + k_2\sum_{i=1}^{N} m_i C_{s,i} + \pi\left(k_2\frac{L\rho_s\phi\sum_{i=1}^{N} f_i A_{s,i}}{\Upsilon} - \sum_{i=1}^{N} k_{12,i}C_d\right), \quad (35)$$

where $C_{s,i}$ and $A_{s,i}$ are, respectively, the concentration of radionuclides in suspended matter and bottom sediments with size $i$ and $\rho_s$ is the sediment bulk density. $\pi = 0$ unless we are solving the equation for the water layer in contact with the sediment. In this case $\pi = 1$ to allow interactions between water and sediments.

The equation that gives the time evolution of specific activity in each of the suspended matter sizes is

$$\frac{\partial(m_i C_{s,i})}{\partial t} + u\frac{\partial(m_i C_{s,i})}{\partial x} + v\frac{\partial(m_i C_{s,i})}{\partial y} + (w - w_{s,i})\frac{\partial(m_i C_{s,i})}{\partial z} = A\left(\frac{\partial^2(m_i C_{s,i})}{\partial x^2} + \frac{\partial^2(m_i C_{s,i})}{\partial y^2}\right) + \frac{\partial}{\partial z}\left(K\frac{\partial(m_i C_{s,i})}{\partial z}\right) + k_{11,i}C_d - k_2 m_i C_{s,i} + \pi(-DPR_i + ERR_i), \quad (36)$$

where $\pi$ has the same meaning as above and $DPR_i$ is the deposition of radionuclides from the deepest water layer to the sediment evaluated according to

$$DPR_i = \frac{w_{s,i} m_i(b) C_{s,i}(b)}{\Upsilon}\left(1 - \frac{\tau_b}{\tau_{cd}}\right). \quad (37)$$

Note that (b) means that the corresponding magnitude is evaluated at the deepest water layer. $ERR_i$ is the resuspension of radionuclides due to sediment erosion

$$ERR_i = \frac{Ef_i A_{s,i}}{\Upsilon}\left(\frac{\tau_b}{\tau_{ce}} - 1\right). \quad (38)$$

Of course, deposition of radionuclides is calculated only if $\tau_b < \tau_{cd}$ and resuspension only if $\tau_b > \tau_{ce}$. Specific activity in the total suspended phase is calculated as

$$C_s^{total} = \frac{\sum_{i=1}^{N} m_i C_{s,i}}{\sum_{i=1}^{N} m_i}. \quad (39)$$

The equation for the temporal evolution of specific activity in each bottom sediment particle size is

$$\frac{\partial A_{s,i}}{\partial t} = k_{12,i}\frac{C_d\Upsilon}{L\rho_s f_i} - k_2 A_{s,i}\phi + DPR_i - ERR_i, \quad (40)$$

where it is remembered that $\Upsilon = \Delta z$ and the deposition and erosion terms are calculated as

$$DPR_i = \frac{w_{s,i} m_i(b) C_{s,i}(b)}{L\rho_s f_i}\left(1 - \frac{\tau_b}{\tau_{cd}}\right), \quad (41)$$

$$ERR_i = \frac{EA_{s,i}}{L\rho_s}\left(\frac{\tau_b}{\tau_{ce}} - 1\right). \quad (42)$$

Total specific activity in bed sediments is calculated from specific activity in each particle size

$$A_s^{total} = \sum_{i=1}^{N} f_i A_{s,i}. \quad (43)$$

### 2.4. Numerical solution

All the equations are solved using explicit finite difference schemes. The scheme described in Flather and Heaps (1975) is used to solve the hydrodynamic equations. For non-linear terms, Scheme 2 described in such reference is used. It consists of calculating changes in components of the horizontal current due to advection alone and adding them to the changes caused by other physical processes computed from the hydrodynamic equations without the advective terms. Although the scheme in Flather and Heaps

(1975) is described for a 2D depth-averaged model, it has been applied to each vertical layer. Additionally, a second-order scheme (see, for instance, Kowalick and Murty, 1993) is used to solve horizontal and vertical diffusion, and the scheme also described in this reference (p. 245) is used for the internal pressure terms.

The MSOU second-order scheme (Vested et al., 1996) is used to solve the advection terms in all the dispersion equations (salinity, suspended matter, radionuclides) and a second-order scheme (Kowalick and Murty, 1993) is also used for the diffusion terms.

Density gradients are calculated using $\sigma_\theta = \rho_w - 1000$ instead of the density (Kowalick and Murty, 1993). Also, the stability of the water column is checked each time step and over all the model domain. Mixing is carried out, using the algorithm described in Kowalick and Murty (1993), when it becomes unstable. The hydrodynamic calculations are started from rest and an uniform salinity of 38 g/L is assumed. The effect of the large-scale circulation can be neglected in the area under study (Marsaleix et al., 1998), as well as tidal currents, that are practically non-existent (Marsaleix et al., 1998; Tsimplis et al., 1995). Indeed, $M_2$ currents are below 1 cm/s in most parts of the Mediterranean and $S_2$ currents have smaller amplitudes.

Open boundary conditions must also be given for suspended matter particles and radionuclides. The open boundary condition described in Periáñez (1999) and Periáñez (2000) has been adopted

$$C_i = \psi C_{i-1}, \tag{44}$$

where $C_i$ represents the concentration of suspended matter and radionuclides along the boundary and $C_{i-1}$ represents the concentration just inside the computational domain. The non-dimensional value of $\psi$ is obtained from a calibration exercise.

The hydrodynamic model is run for a given water discharge from the Rhone until a steady salinity and current amplitude pattern is obtained. Then the suspended matter model is run using such water circulation. The suspended matter model (without the erosion term) is started from a sea bottom containing no sediments. Then the accumulation of particles of each size is calculated to have a first estimation of the distribution of sediment particle sizes over the model domain. Next, the suspended matter model is started (with erosion) from the estimated particle size distribution until a steady state is reached. This way a self-consistent distribution of different particle sizes on the sea bed over the model domain can be obtained. It is assumed that all suspended and surficial sediments originate from the Rhone. This distribution is relevant to calculate the adsorption of radionuclides by the bed sediments.

Once the water circulation, salinity distribution, suspended matter distribution for each particle size and distribution of particles in bed sediments are known and stored in files, the radionuclide dispersion model may be run using these files as input data.

The model domain is presented in Fig. 1. The model resolution is $\Delta x = \Delta y = 1000$ m. A variable grid is used in the vertical to have enough resolution to solve the salinity gradients in the surface plume. Thus, 10 layers with $\Delta z = 1$ m are used followed by thicker layers increasing to $\Delta z = 15$ m. Time step is fixed as 5 s to solve the hydrodynamic equations due to the CFL stability condition. It is increased to 60 s to solve the suspended matter and radionuclide equations. However, when the radionuclide dispersion model was applied to plutonium, time step had to be decreased to 10 s since the following stability condition is introduced by the terms describing

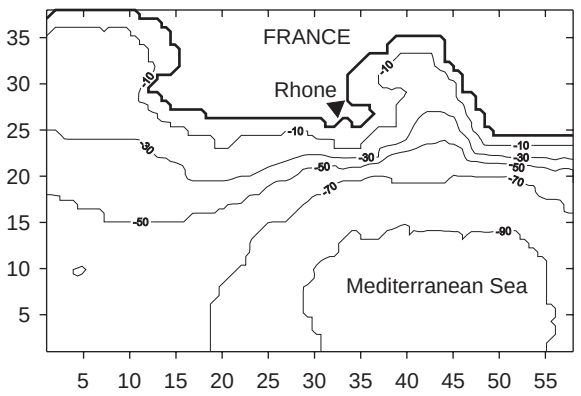


Fig. 1. Model domain. Each unit in the $x$- and $y$-axis is 1000 m. Depths are given in m.

the transfers between the liquid and the solid phases

$$\Delta t < \frac{1}{k_{max}}, \tag{45}$$

where $k_{max}$ is the maximum kinetic rate involved in the equations. It means that the activity transferred from one phase to another in a time step must be smaller than the activity content in the origin phase. This condition is more restrictive for a highly reactive radionuclide as Pu than for more conservative ones as, for instance, Cs.

## 3. Model application and results

Values to the different parameters in the model must be given, as well as the appropriate source terms for suspended matter particles and radionuclides. The bed friction coefficient has been fixed as $k = 0.015$ and the horizontal diffusivity as $A = 20\,\mathrm{m}^2/\mathrm{s}$. The roughness lengths of the sea surface and bottom have been defined as $z_s = z_0 = 0.0034\,\mathrm{m}$. These values are similar to those used by Xing and Davies (1999). The thickness of the freshwater layer discharged from the Rhone is 2 m (Broche et al., 1998) and the width of the river mouth has been fixed as $d = \Delta x = 1000\,\mathrm{m}$, which is very close to reality. Indeed, this approach has already been used in Marsaleix et al. (1998). As commented before, large-scale circulation and tides can be neglected in the area.

The hydrodynamic model has been run for the average discharge from the Rhone River, $1700\,\mathrm{m}^3/\mathrm{s}$ (Broche et al., 1998; Thill et al., 2001), and without wind. The computed water circulation and salinity and viscosity distributions are stored in files that will be used to calculate the suspended matter distribution, deposition rates and the dispersion of radionuclides.

Wind conditions affect the extension and shape of the plume (Estournel et al., 1997, 2001). Two types of winds are predominant in the region: northwest winds (representing 45% of winds exceeding 10 m/s on average over the year) and southeast winds (20% of winds exceeding 10 m/s). The plume response to winds has been studied in the references given above. Although wind stress is formally included in the hydrodynamic equations, the main difficulty in the present work is that observed sedimentation rates, the distribution of different particle classes over the bed and measured radionuclide concentrations in bed sediments integrate many different wind and river discharge conditions. On the other hand, measured radionuclide concentrations in the water column correspond to the particular conditions during sampling, that, on the other hand, took place over a period of several months (Martin and Thomas, 1990). As a consequence, it was decided to run the hydrodynamic model for average discharge from the Rhone River and without wind. This may be a too simple approach, but can give a realistic view of the main dispersion processes in the plume, given the generally good agreement obtained between computations and measurements. Nevertheless, the sensitivity of radionuclide transport in the plume to changing winds and river discharge is an interesting problem that has to be addressed in the next future.

The computed currents in the domain for these conditions are presented in Fig. 2. These currents were obtained after a simulation time of 48 h. This pattern is in agreement with the earlier calculations in Estournel et al. (1997), Marsaleix et al. (1998) and Arnoux-Chiavassa (1998). Water discharged by the river moves in a southeast direction and then rotates towards the west due to Coriolis acceleration and moves along the coast. Broche et al. (1998) released a surface drifter 2 km south

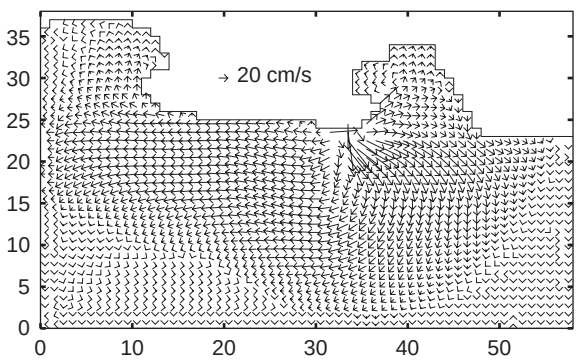


Fig. 2. Computed currents for average water discharge ($1700\,\mathrm{m}^3/\mathrm{s}$) and no wind.

from the river mouth and measured its langrangian velocity during several hours. The movement of a surface drifter has been simulated with the model for the same conditions of the experiment in Broche et al. (1998), water discharge equal to 2000 $m^3/s$ and no wind. A comparison between the observed and computed langrangian velocity of the drifter is presented in Fig. 3. It can be seen that there is a good agreement between both sets of data, indicating that the model is giving a realistic representation of currents in the Rhone plume.

The salinity distribution in the surface plume can be seen in the map presented in Fig. 4a. This distribution is essentially the same as that previously computed in Arnoux-Chiavassa (1998), Estournel et al. (1997) and Marsaleix et al. (1998). The shape of the salinity contours, together with the currents presented in Fig. 2, indicate that the plume forms a bulge of anticyclonic circulation in front of the river mouth. The circulation in the plume is almost entirely baroclinic, that is, induced by the density differences.

A vertical salinity profile following a north–south transect in front of the river mouth can be seen in Fig. 4b. It can be seen that the freshwater is diluted with seawater due to turbulence and upwelling movements, which produce the thinning of the plume that can be appreciated in Fig. 4b. This is in agreement with the earlier computations in Marsaleix et al. (1998).

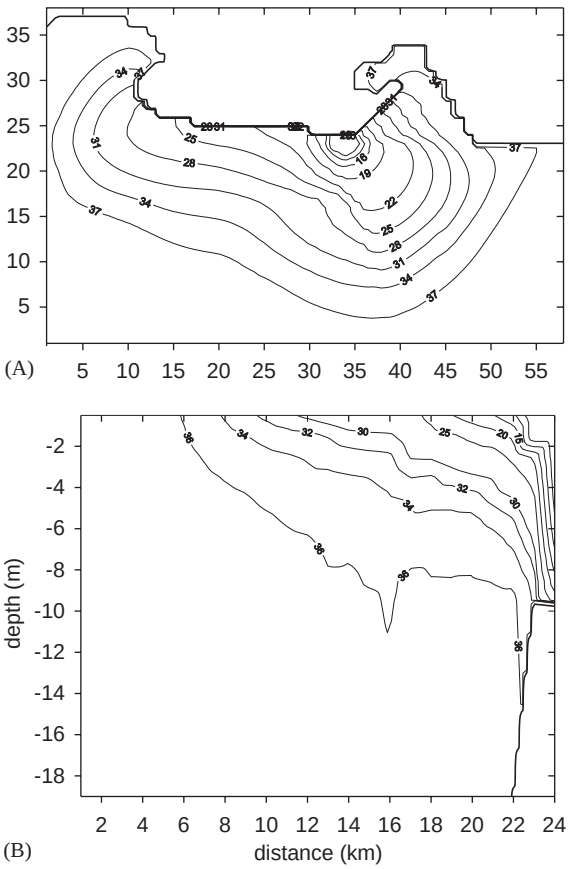


Fig. 4. (A) Computed surface salinity (psu) after a simulation time of 48 h. (B) Computed salinity (psu) south–north profile in front of the river mouth (located 24 km north from the south of the model domain) after a simulation time of 48 h.

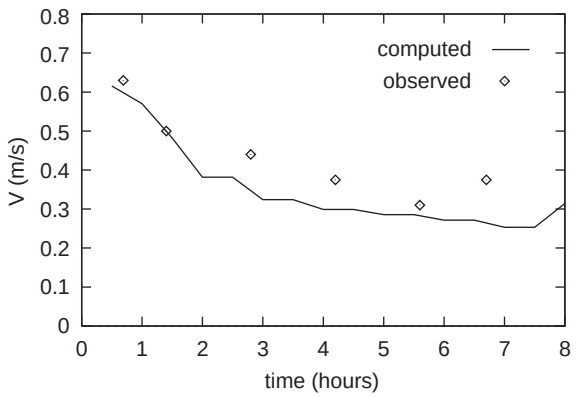


Fig. 3. Observed and computed lagrangian velocities of a surface drifter released 2 km south from the river mouth.

The average suspended matter discharge of the Rhone River is about 4.6 Mt/year, which represents the major particle input into the western Mediterranean Sea. However, the solid discharge has a relevant annual variability, with most of the solids being discharged during flood events. Thomas (1997) has established a correlation for the suspended matter concentration in the river vs. water flow. If such correlation is applied to the average water discharge (1700 $m^3/s$), a suspended matter concentration in the river of 28 mg/L is obtained. This will be the suspended matter source term used in the model. This estimation is in agreement with measurements. For instance, Garnier et al. (1991) measured a suspended load

of 17.6 mg/L for a water discharge of 1600 $m^3/s$; Martin and Thomas (1990) measured 11.3 and 54.0 mg/L for water discharges of 1300 and 2200 $m^3/s$ respectively and Eyrolle et al. (2002) obtained a suspended load of 28.6 mg/L for a water discharge of 1718 $m^3/s$.

Four suspended matter particle sizes are considered in the model according to Thill et al. (2001). These authors measured the proportion of particles of 5 different sizes for low, average and high water discharges. From the total particle concentration given above (28 mg/L) and the measured proportion of particles of each size (for average water discharge), the particle concentration for each size can be calculated. Results are given in Table 1. These concentrations are the boundary conditions of the suspended matter model at the river mouth. The largest particle size has been neglected due to the extremely low proportion in which such particles are present (0.014% of the total). Settling velocities obtained from Stokes's law are also given in Table 1. The threshold deposition stress has been fixed as 0.1 $N/m^2$. This parameter has been observed to be in the range 0.06–1.1 $N/m^2$ (Krone, 1962; Mehta and Partheniades, 1975). After some preliminary calculations without wind, it was found that results were not affected by the erosion term. However, erosion events may be induced by wind waves in the shallower areas. Indeed, waves are the main factor producing sediment erosion in the region (REMOTRANS, 2004). Nevertheless, wave-induced erosion is not included in the model since calculations are carried out under calm conditions (the models of Estournel et al. (1997) and Kondrachoff et al. (1994) do not include sediment erosion although do consider winds).

Table 1
Particle sizes included in the model and their corresponding settling velocities

| Particle size (μm) | $w_s$ (m/s) | $m$ (mg/L) |
|---|---|---|
| 3 | $7.8 \times 10^{-6}$ | 11.5 |
| 7 | $4.2 \times 10^{-5}$ | 9.5 |
| 20 | $3.5 \times 10^{-4}$ | 3.5 |
| 40 | $1.4 \times 10^{-3}$ | 3.5 |

The particle concentration at the Rhone River mouth for average water discharge is also given.

The suspended matter model also provides the distribution of the different particle grain sizes on the sea bed over the model domain (parameter $f_i$ for each particle size), that will be relevant for the calculation of radionuclide concentrations in the bed sediment, as well as provides sedimentation rates over the domain, that can be compared with those derived from observations.

A map showing the total concentration of particles obtained after a computation time of three days can be seen in Fig. 5. The shape and extension of the plume is in qualitative agreement with that obtained from satellite observations (Kondrachoff et al., 1994). The plume is directed to the southwest offshore, following the water circulation. Measured particle concentrations, from Martin and Thomas (1990) and Naudin et al. (2001), are also shown in Fig. 5. As commented before, the particle input from the Rhone depends on the river discharge. Sampling was carried out at different times, thus measured particle concentrations correspond to different source terms. Particle input in the model was estimated from a correlation for the particle concentration in the river mouth vs. river discharge applied to the average discharge. As a consequence, measured

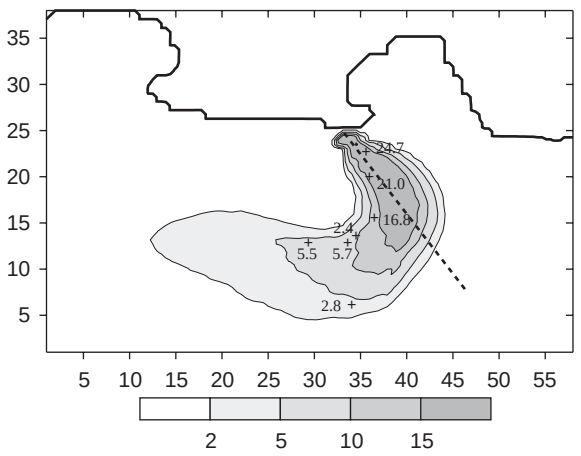


Fig. 5. Computed total suspended matter concentrations (mg/L) over the model domain at the surface after a computation time of 3 days and measured concentrations. The axis of the plume is also shown (dashed line).

concentrations in the plume have been normalized to a mouth particle concentration equal to 28 mg/L (source term in the model) to allow that comparisons between measured and computed concentrations can be carried out. Measured concentrations presented in Fig. 5 are such normalized values.

The suspended particle plume is mainly composed of fine sediments, as the coarser fractions sink close to the river mouth. This can be clearly seen with the help of Fig. 6: coarse particles (20 and 40 μm) soon disappear from the water column as they sink to the sea bed. The largest particles are entirely removed from the water column in less than 5 km, as found by the observations in Thill et al. (2001). The content in particles with size 7 μm decreases to 50% in 10 km, which is similar to the distance of 8 km found in Thill et al. (2001). It can be observed that the content in the smallest particles (3 μm) initially increases, before being finally reduced as the plume is diluted. This increase in surface concentrations of the smallest particles has also been observed in Thill et al. (2001). Several hypothesis were proposed to explain it, like larger particle break-up, primary production, colloid aggregation or simple mixing with a particle-rich saline water source, although none of these mechanisms could clearly explain the behavior of the smallest particles. It seems, however, that the particle increase is a hydrodynamic effect since any other process has not been included in the model.

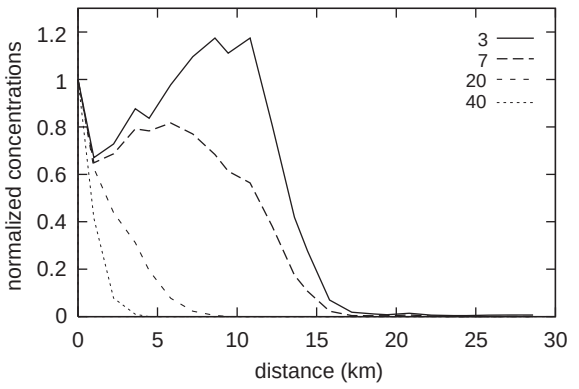


Fig. 6. Computed surface suspended matter concentrations for each particle size along the axis of the plume (see Fig. 5) normalized to the concentrations in the river mouth. Particle sizes are given in μm. Distances are measured respect to the river mouth.

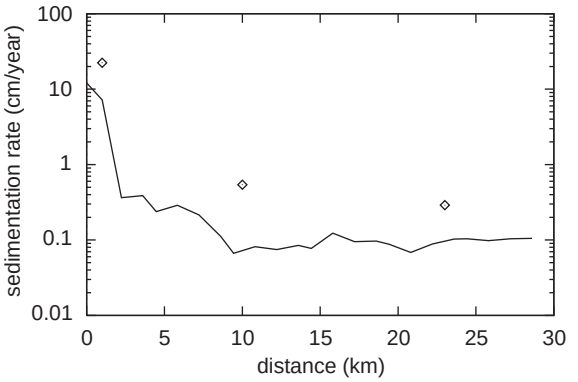


Fig. 7. Computed sedimentation rates along the axis of the plume shown in Fig. 5 (line) together with the values estimated from observations (Radakovitch et al., 1999). Distances are measured respect to the river mouth.

The computed sedimentation rates along the plume axis are shown in Fig. 7 together with the estimations presented in Radakovitch et al. (1999) obtained from $^{210}$Pb profiles. The model underestimates the sedimentation rates. However, the following points have to be considered: firstly, sedimentation rates estimated from observations are maximum possible values since they are calculated assuming that there is no diffusion in the sediment core. Secondly, the values obtained from the model are calculated for an average water discharge, and sedimentation increases after flood events when a large amount of suspended matter is discharged by the river. Finally, if must be taken into account that bed-load transport of coarse material is not included in the model. This process can also contribute to a larger sedimentation rate.

Nevertheless, the model gives a realistic representation of the sedimentation process in the plume. Computed sedimentation rates are similar to those derived by several authors from observations (Radakovitch et al., 1999; Zuo et al., 1997; Charmasson et al., 1998): a deposition belt is observed close to the river mouth, where sedimentation reaches values of the order of 10 cm/year, decreasing on the shelf to values of the order of $10^{-1}$ cm/years. Sedimentation rates suffer a further decrease to values of the order of $10^{-2}$ cm/year when entering the deep-water basin.

Suspended matter concentrations, as well as sedimentation rates, for each particle grain size, are stored in files that will be used by the radionuclide dispersion code together with the current, vertical viscosity and salinity fields generated by the hydrodynamic model.

Radionuclides used in the simulations are $^{125}$Sb, $^{137}$Cs and $^{239+240}$Pu. Sb is considered as a conservative radionuclide, thus $\chi_1 = k_2 = 0$ in this case. Values for the kinetic coefficients have to be defined in the case of Cs and Pu. The exchange velocity depends on water salinity through Eq. (33). The 50% saturation salinity is obtained from the experiments in Laissaoui et al. (1998): $S_0 = 45\,\mathrm{g/L}$. As described in Nyffeler et al. (1984) and also found in the experiments of Laissaoui et al. (1998), $k_2$ is very similar even for radionuclides with a rather different geochemical behavior and it does not seem to be affected by salinity. Thus the value given to $k_2$ is the same that was used in the plutonium dispersion model of the Irish Sea (Periáñez, 1999): $k_2 = 1.16 \times 10^{-5}\,\mathrm{s^{-1}}$. The freshwater value for the exchange velocity has been obtained from the equation relating this parameter with $k_2$ and the freshwater distribution coefficient, $k_d^0$ (Periáñez et al., 1996a)

$$k_d^0 = \frac{\chi_1^0}{k_2}\frac{3}{\rho \overline{R}}, \tag{46}$$

where $\overline{R}$ is the mean radius of suspended matter particles in the river, that has been calculated from the proportion of particles of each size in the river given in Thill et al. (2001). The freshwater value of the distribution coefficients for Cs and Pu has been measured in Martin and Thomas (1990). The following freshwater exchanges velocities have been obtained for Cs and Pu, respectively: $3.80 \times 10^{-6}$ and $5.21 \times 10^{-5}\,\mathrm{m/s}$.

The sediment mixing depth has been fixed as $L = 0.1\,\mathrm{m}$, as in previous modelling works (Periáñez et al., 1996a; Periáñez, 1999). After a calibration process the geometry correction factor is defined as $\phi = 0.1$ and it is used $\psi = 0.99$ in open boundary condition (Eq. (44)). Particles transported by the river have a typical density $\rho = 2600\,\mathrm{kg/m^3}$ (Arnoux-Chiavassa, 1998) and dry density of bed sediments is fixed as $\rho_s = 1600\,\mathrm{kg/m^3}$ (Zuo et al., 1997).

The input of radionuclides from the river has also been obtained from Martin and Thomas (1990), who estimated the radionuclide input to the Mediterranean in dissolved and particulate forms. The input of radionuclides fixed to suspended particles is distributed among the four particle sizes according to the distribution coefficient for each size. This distribution coefficient is calculated by Eq. (46) but replacing $\overline{R}$ by the corresponding particle radius $R_i$. Inputs from the river have been obtained from sampling campaigns carried out in the period 1982–1985. For this time the main source of radionuclides to the river is due to the discharges from Marcoule reprocessing plant, being fallout and watershed soil leaching negligible if compared with them. Also, no relevant discharge variations have been found in these years (Martin and Thomas, 1990). Although short-term variations cannot be assessed, estimations of the inputs to the Mediterranean carried out in Martin and Thomas (1990) provide a realistic reference for the average flux of radionuclides from the Rhone.

The behavior of Pu in aquatic systems is of considerable complexity due to the fact that can exist in different oxidation states simultaneously. The reduced Pu [Pu(III) and Pu(IV)] is highly particle reactive and has been shown to possess a $k_d$ that is approximately two orders of magnitude higher than that of the more soluble oxidized Pu [Pu(V) and Pu(VI)]. Different exchange velocities (obtained from the different $k_d^0$s through Eq. (46)) should be used for oxidized and reduced Pu, as has been done in Periáñez (2003). However, in this work different plutonium oxidation states have not been considered due to the lack of experimental data on Pu speciation in the Rhone area. Thus, measurements (of Pu concentrations and $k_d$s) represent the mixture of oxidation states that is present in the particular sample. A measured effective $k_d^0$, representative of such mixture, is used to obtain an effective exchange velocity. This approach for simulating Pu dispersion is used in other models (Periáñez, 1999; Aldridge et al., 2003).

It has been found that Cs is not significantly fixed to colloids (Eyrolle and Charmasson, 2001). The fraction of colloidal Pu measured by Eyrolle

and Charmasson (2004) ranges from 0 to 41% of the dissolved phase plutonium content. Considering that over 90% of Pu is fixed to suspended matter (see below), the fraction of colloidal Pu represents a maximum of 4% of the total Pu content. Thus, colloids have been neglected in the case of Pu as well. Also, it seems that changes in POC (particulate organic carbon) do not affect significantly the adsorption of radionuclides (Thomas, 1997).

The dispersion of radionuclides released from the river is calculated until a steady distribution is obtained. The radionuclide discharges are carried out assuming that the sea is initially not contaminated. The computed distribution of $^{125}$Sb in surface water is presented in Fig. 8a. As commented above, it is assumed that this radionuclide is conservative, thus it is not fixed to the solid phases.

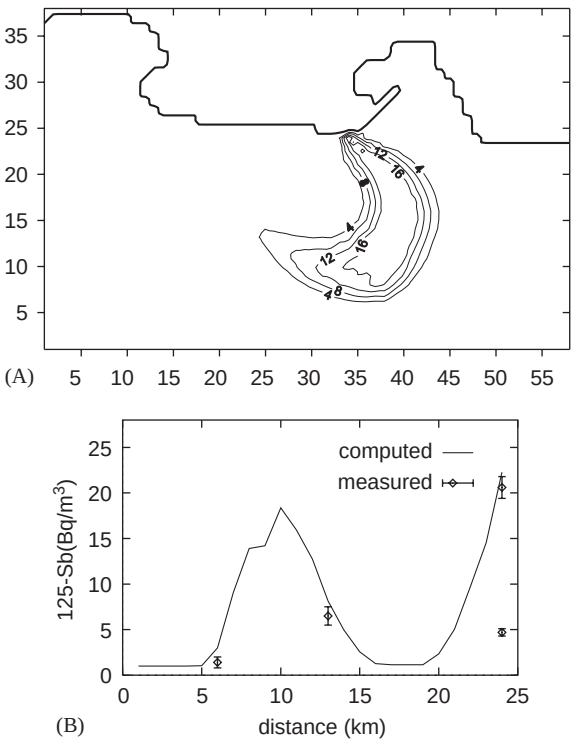


Fig. 8. (A) Computed distribution of $^{125}$Sb (Bq/m$^3$) in surface water due to river discharge. (B) Measured and computed south–north profile of $^{125}$Sb in surface waters in front of the river mouth. Distances are measured from the south of the model domain (the river mouth is at km 24) The computed profile corresponds to river discharge plus an uniform background due to fallout.

The patch of radionuclides follows the water circulation in the plume. It is initially directed to the south and after is deflected to the right in a southwest direction. Model results are compared with observations in Fig. 8b, where south–north profiles of $^{125}$Sb in surface water are presented [the observations have been taken from Martin and Thomas (1990)]. Activity levels are reproduced by the model. The apparent activity peak at km 10 and the minimum around km 18 are due to the curvature of the plume (it can be clearly seen if a south–north profile is plotted in Fig. 8a at $x = 34$). Measured activity levels correspond to the addition of discharges from the river and fallout over the Mediterranean. An uniform activity background, due to atmospheric fallout, has been added to the computed specific activities in order to compare model results with observations. $^{125}$Sb specific activity due to fallout in the Gironde estuary ranges 1.9–2.9 Bq/m$^3$ (Martin and Thomas, 1990) during 1984. Since the maximum measured specific activity is 1.4 Bq/m$^3$ at 18 km to the south of the river mouth (Martin and Thomas, 1990), it has been assumed that this concentration is the background due to fallout in the region (supposing that essentially all activity at this point is due to fallout). This number is similar to background in the Gironde estuary (see above). Thus, specific activities presented in Fig. 8b correspond to the computed specific activities due to river discharges (presented in Fig. 8a) plus an uniform background of 1.4 Bq/m$^3$.

The computed distribution of $^{137}$Cs in water and suspended matter due to discharges from the river is presented in Fig. 9. The dissolved pattern is similar to that of $^{125}$Sb, but a different distribution is found for radionuclides fixed to suspended particles: in this case activity is also transported towards the west along the coast. Model results are compared with observations in Fig. 10, where south–north profiles in front of the river mouth of $^{137}$Cs in water and suspended matter are shown. As in the case of $^{125}$Sb, computed profiles presented here correspond to the input from the river (Fig. 9) plus an uniform background due to atmospheric fallout. Pre-Chernobyl $^{137}$Cs average

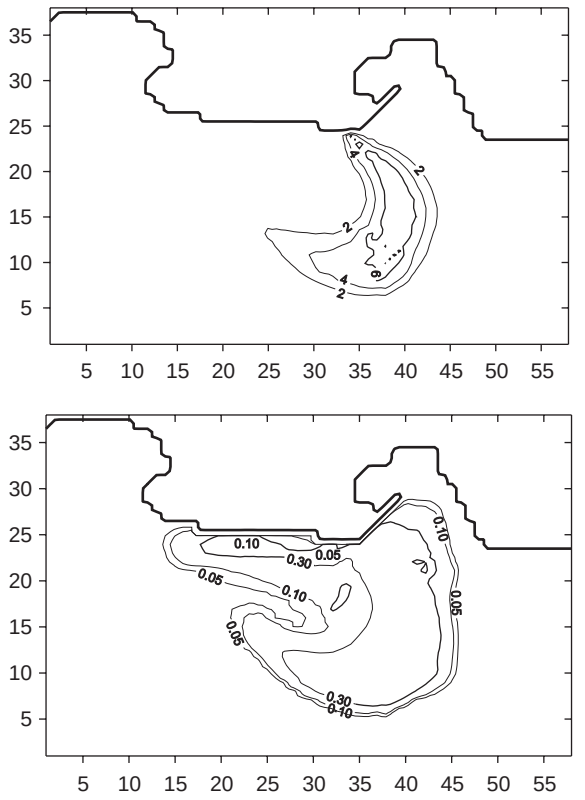


Fig. 9. Computed distributions of $^{137}$Cs in surface water (up), Bq/m$^3$, and suspended matter (down), Bq/g, due to discharges from the river.

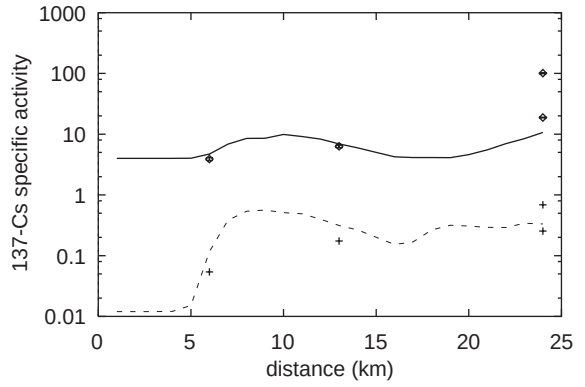


Fig. 10. Measured (points) and computed (lines) south–north profiles of $^{137}$Cs in surface water (solid line, boxes), in Bq/m$^3$, and suspended matter (dashed line, crosses), in Bq/g, in front of the river mouth. Distances are measured from the south of the model domain (the river mouth is at km 24).

specific activities due to fallout in the Mediterranean are 5.4 Bq/m$^3$ (Gascó et al., 2002) during the period 1970–82 and 3.1 Bq/m$^3$ (Martin and Thomas, 1990) during February–April 1986. An intermediate value of 4 Bq/m$^3$ has been used for the dissolved background. From this quantity, and assuming that the distribution of fallout radionuclides between water and suspended particles is at equilibrium, the fallout background in suspended matter is calculated using the equilibrium $k_d$ of $3 \times 10^3$ L/kg given in IAEA (1985). Its value is 0.012 Bq/g. It can be seen in Fig. 10 that the model gives a good representation of activity levels detected in the river plume in both dissolved and particulate forms.

The computed distribution of $^{137}$Cs in bed sediments is presented in Fig. 11, together with observations obtained from Martin and Thomas (1990). It can be seen that the model gives a correct estimation of activity levels in the vicinity of the river mouth, although underestimates them away from it. It must be taken into account that sediments integrate radionuclide input variations over time. Also, episodes of high river discharge, when larger amounts of particles are released to the sea and are also transported to greater distances from the river mouth, are integrated in the measured concentrations. Computed concentrations are obtained for average water, suspended particles and radionuclide discharges. It is not possible to have a accurate agreement between measurements and computations with a model working in *average* conditions. Nevertheless, it

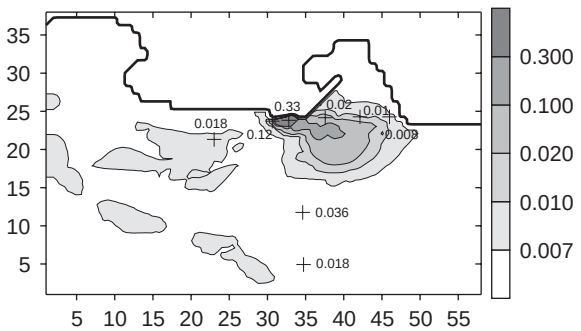


Fig. 11. Computed distribution of $^{137}$Cs in bed sediments (Bq/g). Measured concentrations (Martin and Thomas, 1990) are also shown.

seems clear that the model produces rather realistic activity levels in the area of the river mouth. Indeed, the distribution map in Fig. 11 is very similar to that presented in Charmasson (2003), where a sharp decrease in inventories with distance from the river mouth can be seen. Finally, it must be taken into account that measured bed concentrations include deposition from global fallout. Only sampling stations close to the river mouth in Charmasson (2003) present $^{137}$Cs inventories clearly in excess with respect the cumulative deposit due to global fallout (Chernobyl is not considered since occurred later than the time of our simulations). Thus, most of $^{137}$Cs coming from the river appears in sediments of a well-delimited zone in the close vicinity of the river mouth. Our simulations are in agreement with these findings. Nevertheless, it seems clear that the transport of radionuclides under extreme and changing wind conditions, as well as peak river discharge, needs to be investigated.

The model can also give a wide amount of information, as fractions of radionuclides in suspended matter (for total suspended load and each particle size) and distribution coefficients for suspended matter–water and bed sediment–water systems (also for the total solid phase and each particle size). It is interesting to point out that the model can calculate distribution coefficients instead of requiring them as input data. As an example, the computed fraction of $^{137}$Cs fixed to suspended matter particles in surface waters of the plume is presented in Fig. 12. It can be seen that about 60% is fixed to solid particles. In Eyrolle and Charmasson (2001) it is pointed out that 30% of $^{137}$Cs is transported by the Rhone River in the particulate phase, although this percentage is increased to 83% in Martin and Thomas (1990). Indeed, these authors have found that the particulate phase is the major vector for most of the radionuclides. Calmet and Fernandez (1990) have also found that $^{137}$Cs associated with particles represents 68% of the Rhone input. Thomas (1997) has also found that radionuclide transport in the particulate phase is specially relevant during flood events, when the fraction of radionuclides in particles reaches 0.75–0.99. Computed suspended matter–water distribution coefficients (total suspended matter) for surface waters are also presented in Fig. 12. They are of the order of $10^4$ L/kg in the area of the river plume, decreasing in one order of magnitude out of it and approaching the average value recommended by IAEA (1985) for Cs ($3 \times 10^3$). This behavior may be similar to that observed (Mitchell et al., 1995) in the Irish Sea for Pu [and also reproduced by a model (Periáñez, 1999)], where distribution coefficients decrease when increasing distance from Sellafield. It was attributed to the nature of discharges since virtually all plutonium was released in particulate form (Mitchell et al., 1995). The same situation is presented in the plume since most $^{137}$Cs is released in particulate form. However, the decrease in the exchange velocity with salinity included in the model (Eq. (33)) will also produce a decrease in the

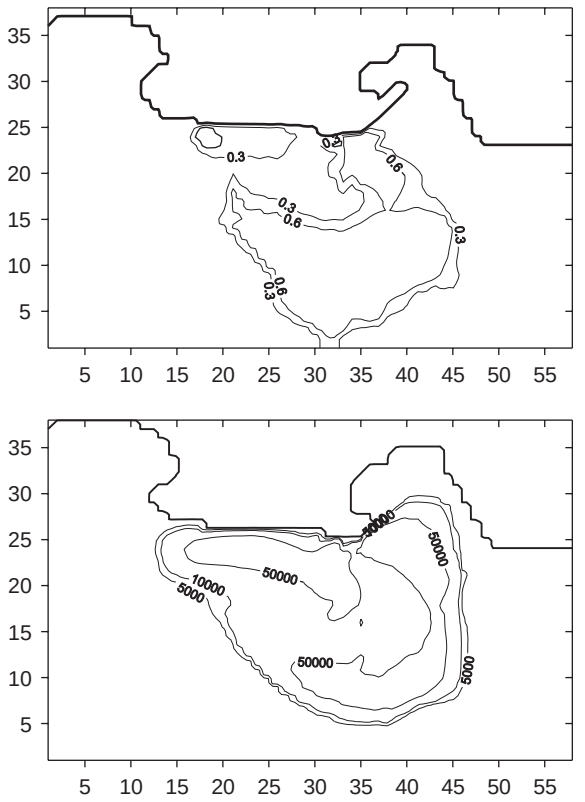


Fig. 12. Computed $^{137}$Cs fraction fixed to suspended particles in surface waters (up) and computed suspended matter–water $k_d$ (L/kg) in surface waters (down).

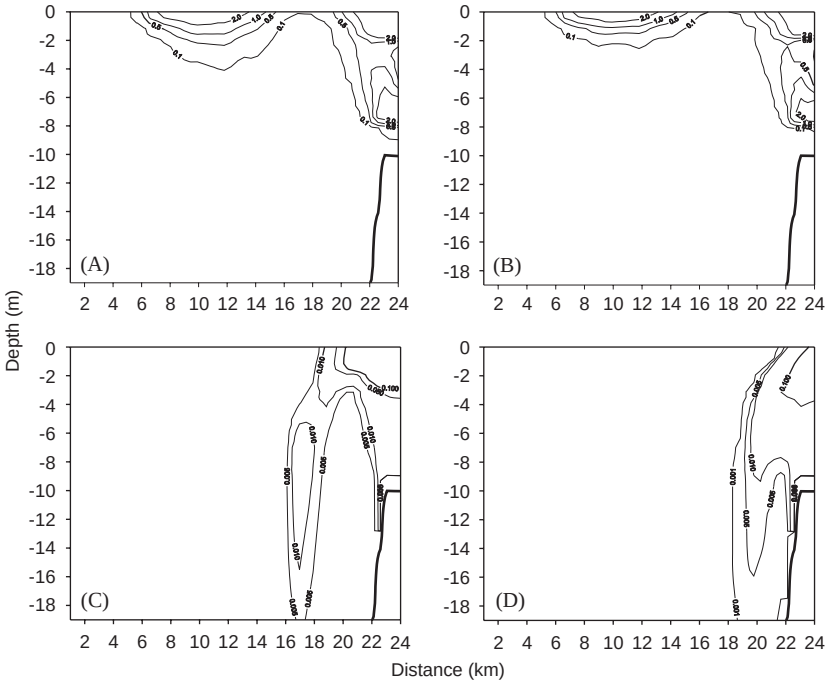


Fig. 13. Computed $^{137}$Cs activity in suspended matter in Bq/m$^3$ for a south–north vertical profile in front of the river mouth. (A) total suspended matter. (B), (C) and (D) 3, 20 and 40 μm particles, respectively. Distances are measured from the south of the model domain. The river mouth is at km 24.

distribution coefficients as distance from the river mouth increases and, consequently, salinity increases too.

South–north vertical profiles of specific activity in suspended matter in front of the river mouth and for several particle sizes are presented in Fig. 13, together with specific activity in total suspended load. It can be seen that the radionuclide content in the plume suspended load is essentially controlled by the smallest particles, since Figs. 13a and b are very similar. Coarse particles quickly sink to the bottom and, as a consequence, radionuclides are only present in a small region in front of the river mouth as can be seen in Figs. 13c and d. This is in agreement with the results of Martin and Thomas (1990), who found a deposition belt close to the river mouth. It seems that this deposition belt is produced by the coarsest particles in the plume.

Calmet and Fernandez (1990) have measured a decrease in $^{137}$Cs activity with increasing depth in the water column. Such decrease has also been

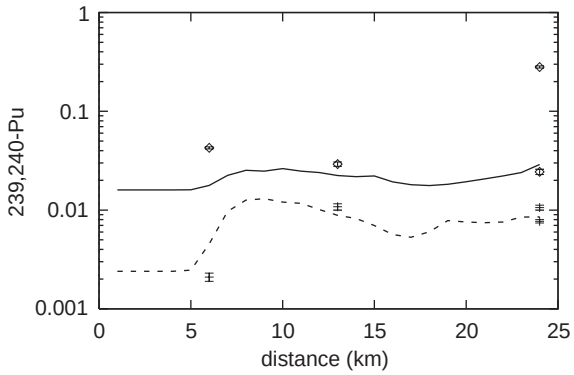


Fig. 14. Measured (points) and computed (lines) south–north profiles of $^{239,240}$Pu in surface water (solid line, boxes), in Bq/m$^3$, and suspended matter (dashed line, crosses), in Bq/g, in front of the river mouth. Distances are measured from the south of the model domain (the river mouth is at km 24).

produced by the model although numbers cannot be directly compared since measurements include the input of radionuclides from the Rhone plus

Chernobyl fallout and the model does not account for the last.

A comparison of model results with measurements for the application to $^{239,240}$Pu is presented in Fig. 14, where south–north plutonium profiles in water and suspended matter in front of the river mouth are shown. Plutonium fallout backgrounds have been added to the specific activities calculated by the model, which correspond to the input from the river only. Specific activity in water due to fallout plutonium is 0.016 Bq/m$^3$ (Martin and Thomas, 1990). Using the Pu $k_d$ value measured in the northwestern Mediterranean (Molero et al., 1995), $1.4 \times 10^5$ L/kg, which is also in good agreement with the average value of the Pu distribution coefficient in coastal waters recognized in IAEA (1985), $1.0 \times 10^5$ L/kg, the specific activity in suspended matter particles due to fallout plutonium (again assuming equilibrium for fallout radionuclides) is 0.0024 Bq/g. It can be seen that the model gives a correct estimation of plutonium levels in both phases in the river plume. These activity levels are two orders of magnitude lower than those of $^{137}$Cs due to the smaller Pu input rate. The fraction of plutonium at the surface fixed to the suspended particulate phase is given in Fig. 15. It can be seen that over 90% of Pu in the plume is attached to particles. This is in agreement with Thomas (1997), who found that plutonium predominates in particulate form in most hydrological conditions, and with Eyrolle and Charmasson (2004), who have reported that

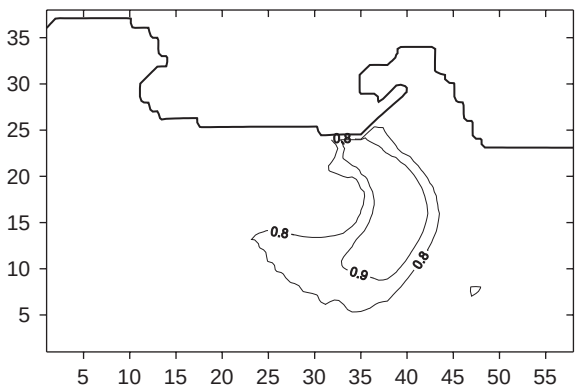


Fig. 15. Computed $^{239,240}$Pu fraction fixed to suspended particles in surface waters.

85% of Pu isotopes are bound to particles in the river. Computed distribution coefficients in the plume are of the order of $3 \times 10^5$ L/kg, decreasing out of it and approaching the value found by Molero et al. (1995). The general behavior is similar to that of $^{137}$Cs.

## 4. Conclusions

A full 3D model has been developed to simulate the transport of radionuclides in a river plume. Currents are almost entirely baroclinic (induced by water density differences). Thus, the hydrodynamic model must include the terms accounting for such density differences in the equations and must also have a vertical resolution high enough to solve the pycnocline. A turbulence model has also been coupled to provide the vertical eddy viscosity.

Together with the hydrodynamic equations, the model solves the suspended matter dynamics. Several suspended particle sizes have been included, since model output is rather sensitive to this parameter and the size spectra of particles discharged by a river is generally wide. The effect of salinity on uptake kinetics has finally been included. The model provides a wide amount of information, as horizontal distributions and vertical profiles of specific activities in water, total suspended matter and each suspended particle size, percentages of radionuclides in total suspended matter and each particle size, distribution coefficients for total suspended matter and each particle size and distribution of radionuclides in bed sediments, for the total sediment and each particle size.

The model has been applied to simulate the transport of $^{137}$Cs, $^{125}$Sb and $^{239+240}$Pu in the Rhone River plume. The computed water circulation and salinity pattern is, in general, in agreement with observations and earlier hydrodynamic models. Four suspended matter particle sizes have been considered in the model. It gives a realistic representation of the behavior of the different particle sizes in the plume, as well as of the sedimentation processes. Model results for radionuclide dispersion are, in general, in good agreement with observations. Thus, it seems that the

processes included in the model have been adequately described. Nevertheless, as already commented, the effect of dynamic winds and changing river flows on radionuclide transport in the plume has to be addressed in the next future.

## Acknowledgements

Work supported by ENRESA and EU 5th Framework Programme (1998–2002) Nuclear Fission and Radiation Protection Contract FIGE-CT-2000-00085.

## References

Abril, J.M., García-León, M., 1993. A 2D 4-phases marine dispersion model for non conservative radionuclides, Part 1: conceptual and computational model. Journal of Environmental Radioactivity 20, 71–88.

Aldridge, J.N., Kershaw, P., Brown, J., McCubbin, D., Leonard, K.S., Young, E.F., 2003. Transport of plutonium ($^{239/240}$Pu) and caesium ($^{137}$Cs) in the Irish Sea: comparison between observations and results from sediment and contaminant transport modelling. Continental Shelf Research 23, 869–899.

Arnoux-Chiavassa, S., 1998. Modelisation d'ecoulements cotiers stratifies presentant des fronts: application au panache du Rhone. Ph.D. Thesis, University of Toulon.

Broche, P., Devenon, J.L., Forget, P., Maistre, J.J., Naudin, J.J., Cauwet, G., 1998. Experimental study of the Rhone plume, Part 1: physics and dynamics. Oceanologica Acta 21, 725–738.

Calmet, D., Fernandez, J.M., 1990. Caesium distribution in northwest Mediterranean seawater, suspended particles and sediments. Continental Shelf Research 10, 895–913.

Cancino, L., Neves, R., 1999. Hydrodynamic and sediment suspension modelling in estuarine systems, Part I: description of the numerical models. Journal of Marine Systems 22, 105–116.

Clarke, S., 1995. Advective/diffusive processes in the Firth of Forth. Ph.D. Thesis. University of Wales, Bangor, UK.

Clarke, S., Elliott, A.J., 1998. Modelling suspended sediment concentrations in the Firth of Forth. Estuarine, Coastal and Shelf Science 47, 235–250.

Charmasson, S., 2003. $^{137}$Cs inventory in sediment near the Rhone mouth: role played by different sources. Oceanologica Acta 26, 435–441.

Charmasson, S., Bouisset, P., Radakovitch, O., Pruchon, A.S., Arnaud, M., 1998. Long core profiles of $^{137}$Cs, $^{134}$Cs, $^{60}$Co and $^{210}$Pb in sediment near the Rhone River (northwestern Mediterranean Sea). Estuaries 21, 367–378.

Cugier, P., Le Hir, P., 2002. Development of a 3D hydrodynamic model for coastal ecosystem modelling. Application to the plume of the Seine River. Estuarine, Coastal and Shelf Science 55, 673–695.

Davies, A., Hall, P., 2000. A three dimensional model of diurnal and semidiurnal tides and tidal mixing in the North Channel of the Irish Sea. Journal of Geophysical Research 105, 17079–17104.

Eisma, D., 1993. Suspended Matter in the Aquatic Environment. Springer, Berlin.

Estournel, C., Kondrachoff, V., Marsaleix, P., Vehil, R., 1997. The plume of the Rhone: numerical simulation and remote sensing. Continental Shelf Research 17, 899–924.

Estournel, C., Broche, P., Marsaleix, P., Deveneon, J.L., Auclair, F., Vehil, R., 2001. The Rhone River plume in unsteady conditions: numerical and experimental results. Estuarine, Coastal and Shelf Science 53, 25–38.

Eyrolle, F., Charmasson, S., 2001. Distribution of organic carbon, selected stable elements and artificial radionuclides among dissolved, colloidal and particulate phases in the Rhone River (France): preliminary results. Journal of Environmental Radioactivity 55, 145–155.

Eyrolle, F., Charmasson, S., 2004. Importance of colloids in the transport within the dissolved phase (<450 nm) of artificial radionuclides from the Rhone River towards the Gulf of Lions (Mediterranean Sea). Journal of Environmental Radioactivity 72, 273–286.

Eyrolle, F., Arnaud, M., Duffa, C., Renaud, P., 2002. Plutonium fluxes from the Rhone River to the Mediterranean Sea. Radioprotection Colloques 37, 87–92.

Flather, R.A., Heaps, N.S., 1975. Tidal computations for Morecambe Bay. Geophysical Journal of the Royal Astronomical Society 42, 489–517.

Garnier, J.M., Martin, J.M., Mouchel, J.M., Thomas, A.J., 1991. Surface reactivity of the Rhone suspended matter and relation with trace element sorption. Marine Chemistry 36, 267–289.

Gascó, C., Antón, M.P., Delfanti, R., González, A.M., Meral, J., Pappuci, C., 2002. Variation of the activity concentrations and fluxes of natural ($^{210}$Po, $^{210}$Pb) and anthropogenic radionuclides ($^{239,240}$Pu, $^{137}$Cs) in the Strait of Gibraltar (Spain). Journal of Environmental Radioactivity 62, 241–262.

Goshawk, J.A., Clarke, S., Smith, C.N., McDonald, P., 2003. MEAD (Part 1)-a mathematical model of the long-term dispersion of radioactivity in shelf sea environments. Journal of Environmental Radioactivity 68, 115–135.

Gurbutt, P.A., Kershaw, P.J., Durance, J.A., 1988. Modelling the distribution of soluble and particle adsorbed radionuclides in the Irish Sea. In: Guary, J.C., Guegueniat, P., Pentreath, R.J. (Eds.), Radionuclides: A Tool for Oceanography. Elsevier, Amsterdam, pp. 395–407.

Holt, J.T., James, I.D., 1999. A simulation of the southern North Sea in comparison with measurements from the North Sea Project. Part 2: suspended particulate matter. Continental Shelf Research 19, 1617–1642.

IAEA, 1985. Sediment $k_d$ and concentration factors for radionuclides in the marine environment. Technical Report Series 247, Vienna.

Jiang, W., Pohlmann, T., Sundermann, J., Feng, S., 2000. A modelling study of SPM transport in the Bohai Sea. Journal of Marine Systems 24, 175–200.

Kondrachoff, V., Estournel, C., Marsaleix, P., Vehil, R., 1994. Detection of the Rhone River plume using NOAA-AVHRR data. Comparison with hydrodynamic modeling results. Oceanic Remote Sensing and Sea Ice Monitoring 2319, 73–84.

Kowalick, Z., Murty, T.S., 1993. Numerical Modelling of Ocean Dynamics. World Scientific, Singapore.

Krone, R.B., 1962. Flume studies of the transport of sediment in estuarine shoaling processes. Final Report to the San Francisco District US Army Corps of Engineers. University of California, Berkeley.

Laissaoui, A., Abril, J.M., Periánez, R., García-León, M., García-Montaño, E., 1998. Determining kinetic transfer coefficients for radionuclides in estuarine waters: reference values for $^{133}$Ba and effects of salinity and suspended load concentrations. Journal of Radioanalytical Nuclear Chemistry 237, 55–61.

Liu, W.C., Hsu, M.H., Kuo, A.Y., 2002a. Modelling of hydrodynamics and cohesive sediment transport in Tanshui River estuarine system, Taiwan. Marine Pollution Bulletin 44, 1076–1088.

Liu, J.T., Chao, S., Hsu, R.T., 2002b. Numerical modeling study of sediment dispersal by a river plume. Continental Shelf Research 22, 1745–1773.

Lumborg, U., Windelin, A., 2003. Hydrography and cohesive sediment modelling: application to the Romo Dyb tidal area. Journal of Marine Systems 38, 287–303.

Luyten, P.J., Deleersnijder, E., Ozer, J., Ruddick, K.G., 1996. Presentation of a family of turbulence closure models for stratified shallow water flows and preliminary application to the Rhine outflow region. Continental Shelf Research 16, 101–130.

Margvelashvily, N., Maderich, V., Zheleznyak, M., 1999. Simulation of radionuclide fluxes from the Dnieper-Bug estuary into the Black Sea. Journal of Environmental Radioactivity 43, 157–171.

Marsaleix, P., Estournel, C., Kondrachoff, V., Vehil, R., 1998. A numerical study of the formation of the Rhone River plume. Journal of Marine Systems 14, 99–115.

Martin, J.M., Thomas, A.J., 1990. Origins, concentrations and distributions of artificial radionuclides discharged by the Rhone River to the Mediterranean Sea. Journal of Environmental Radioactivity 11, 105–139.

McKay, W.A., Walker, M.I., 1990. Plutonium and americium behavior in Cumbria near shore waters. Journal of Environmental Radioactivity 12, 267–283.

Mehta, A.J., 1989. On estuarine cohesive sediment suspension behavior. Journal of Geophysical Research 94 (C10), 14303–14314.

Mehta, A.J., Partheniades, E., 1975. An investigation of the depositional properties of flocculated fine sediments. Journal of Hydraulic Research 12, 361–381.

Mitchell, P.I., Vives i Batlle, J., Downes, A.B., Condren, O.M., León-Vintró, L., Sánchez-Cabeza, J.A., 1995. Recent observations on the physico chemical speciation of plutonium in the Irish Sea and the western Mediterranean. Applied Radiation and Isotopes 46, 1175–1190.

Molero, J., Sánchez-Cabeza, J.A., Merino, J., Vives Batlle, J., Mitchell, P.I., Vidal-Cuadras, A., 1995. Particulate distribution of plutonium and americium in surface waters from the Spanish Mediterranean coast. Journal of Environmental Radioactivity 28, 271–283.

Nakano, M., Povinec, P., 2003. Modelling the distribution of plutonium in the Pacific Ocean. Journal of Environmental Radioactivity 69, 85–106.

Naudin, J.J., Cauwet, G., Fajon, C., Oriol, L., Terzic, S., Devenon, J.L., Broche, P., 2001. Effect of mixing on microbial communities in the Rhone River plume. Journal of Marine Systems 28, 203–227.

Nicholson, J., O'Connor, B.A., 1986. Cohesive sediment transport model. Journal of Hydraulic Engineering 112, 621–640.

Nielsen, S.P., 1995. A box model for North-East Atlantic coastal waters compared with radioactive tracers. Journal of Marine Systems 6, 545–560.

Nielsen, S.P., Iosjpe, M., Strand, P., 1997. Collective doses to man from dumping of radioactive waste in the Artic Seas. The Science of the Total Environment 202, 135–146.

Nyffeler, U.P., Li, Y.H., Santschi, P.H., 1984. A kinetic approach to describe trace element distribution between particles and solution in natural aquatic systems. Geochimica Cosmochimica Acta 48, 1513–1522.

Orlanski, I., 1976. A simple boundary condition for unbounded hyperbolic flows. Journal of Computational Physics 21, 255–261.

Periáñez, R., 1999. Three dimensional modelling of the tidal dispersion of non conservative radionuclides in the marine environment. Application to $^{239,240}$Pu dispersion in the eastern Irish Sea. Journal of Marine Systems 22, 37–51.

Periáñez, R., 2000. Modelling the tidal dispersion of $^{137}$Cs and $^{239,240}$Pu in the English Channel. Journal of Environmental Radioactivity 49, 259–277.

Periáñez, R., 2002. The enhancement of $^{226}$Ra in a tidal estuary due to the operation of fertilizer factories and redissolution from sediments: experimental results and a modelling study. Estuarine, Coastal and Shelf Science 54, 809–819.

Periáñez, R., 2003. Kinetic modelling of the dispersion of plutonium in the eastern Irish Sea: two approaches. Journal of Marine Systems 38, 259–275.

Periáñez, R., 2004a. Testing the behavior of different kinetic models for uptake/release of radionuclides between water and sediments when implemented in a marine dispersion model. Journal of Environmental Radioactivity 71, 243–259.

Periáñez, R., 2004b. On the sensitivity of a marine dispersion model to parameters describing the transfers of radionuclides between the liquid and solid phases. Journal of Environmental Radioactivity 73, 101–115.

Periáñez, R., Martínez-Aguirre, A., 1997. U and Th concentrations in an estuary affected by phosphate fertilizer processing: experimental results and a modelling study. Journal of Environmental Radioactivity 35, 281–304.

Periáñez, R., Abril, J.M., García-León, M., 1996a. Modelling the dispersion of non conservative radionuclides in tidal waters, Part 2: application to $^{226}$Ra dispersion in an estuarine system. Journal of Environmental Radioactivity 31, 253–272.

Periáñez, R., Abril, J.M., García-León, M., 1996b. Modelling the dispersion of non conservative radionuclides in tidal waters, Part 1: conceptual and mathematical model. Journal of Environmental Radioactivity 31, 127–141.

Piasecki, M., 1998. Transport of radionuclides incorporating cohesive/non cohesive sediments. Journal of Marine Environmental Engineering 4, 331–365.

Prandle, D., 1984. A modelling study of the mixing of $^{137}$Cs in the seas of the European continental shelf. Philosophical Transactions of the Royal Society, London, A 310, 407–436.

Prandle, D., Hargreaves, J.C., McManus, J.P., Campbell, A.R., Duwe, K., Lane, A., Mahnke, P., Shimwell, S., Wolf, J., 2000. Tide, wave and suspended sediment modelling on an open coast, Holderness. Coastal Engineering 41, 237–267.

Radakovitch, O., Charmasson, S., Arnaud, M., Bouisset, P., 1999. $^{210}$Pb and caesium accumulation in the Rhone Delta sediments. Estuarine, Coastal and Shelf Science 48, 77–92.

REMOTRANS, 2004. Processes regulating remobilisation, bioavailability, and translocation in marine sediments. EU Project FIS5-1999-00279 Remotrans 000509, Final Report.

Ruddick, K.G., Deleersnijder, E., Luyten, P.J., Ozer, J., 1995. Haline stratification in the Rhine–Meuse freshwater plume: a three dimensional model sensitivity analysis. Continental Shelf Research 15, 1597–1630.

Salomon, J.C., Breton, M., Guegueniat, P., 1995. A 2D long term advection dispersion model for the Channel and southern North Sea. Part B: transit time and transfer function from La Hague. Journal of Marine Systems 6, 515–527.

Scott, E.M., 2003. Modelling Radioactivity in the Environment. Elsevier, Amsterdam.

Segschneider, J., Sundermann, J., 1998. Simulating large scale transport of suspended matter. Journal of Marine Systems 14, 81–97.

Smith, C.N., Goshawk, J.A., Charles, K., McDonald, P., Leonard, K.S., McCubbin, D., 2003. MEAD (part II)—predictions of radioactivity concentrations in the Irish Sea. Journal of Environmental Radioactivity 68, 193–214.

Tattersall, G.R., Elliott, A.J., Lynn, N.M., 2003. Suspended sediment concentrations in the Tamar estuary. Estuarine, Coastal and Shelf Science 57, 679–688.

Thiessen, K.M., Thorne, M.C., Maul, P.R., Prohl, G., Wheater, H.S., 1999. Modelling radionuclide distribution and transport in the environment. Environmental Pollution 100, 151–177.

Thill, A., Moustier, S., Garnier, J.M., Estournel, C., Naudin, J.J., Bottero, J.Y., 2001. Evolution of particle size and concentration in the Rhone River mixing zone: influence of salt flocculation. Continental Shelf Research 21, 2127–2140.

Thomas, A.J., 1997. Input of artificial radionuclides to the Gulf of Lions and tracing the Rhone influence in marine surface sediments. Deep Sea Research II 44, 577–595.

Tsimplis, M.N., Proctor, R., Flather, R.A., 1995. A two-dimensional tidal model for the Mediterranean Sea. Journal of Geophysical Research 100, 223–239.

Vested, H.J., Baretta, J.W., Ekebjærg, L.C., Labrosse, A., 1996. Coupling of hydrodynamical transport and ecological models for 2D horizontal flow. Journal of Marine Systems 8, 255–267.

Wu, Y., Falconer, R.A., Uncles, R.J., 1998. Modelling of water flows and cohesive sediment fluxes in the Humber Estuary, UK. Marine Pollution Bulletin 37, 182–189.

Xing, J., Davies, A., 1999. The effect of wind direction and mixing upon the spreading of a bouyant plume in a non-tidal regime. Continental Shelf Research 19, 1437–1483.

Zuo, Z., Eisma, D., Gieles, R., Beks, J., 1997. Accumulation rates and sediment deposition in the northwestern Mediterranean. Deep Sea Research II 44, 597–609.